Electronic Supplementary Information

Massive Amplification of Photoluminescence and Exceptional Water Stability of $MAPbBr_3$ Nanocrystals through Core-Shell Nanostructure formation in a Self-Defense Mechanism

Shovon Chatterjee, Tanmoy Khan, Arghya Sen, Nilimesh Das,* and Pratik Sen*

Department of Chemistry, Indian Institute of Technology Kanpur, Kanpur – 208 016, UP, India

Contents

Section S1: Characterization of green solvent medium

Section S2: Reusability of the green solvent medium

Section S3: Characterization of oleylammonium halide salts

Section S4: Photoluminescence quantum yield calculation

Section S5: Powder X-ray diffraction studies

Section S6: X-ray photoelectron spectroscopy studies

Section S7: Microscopic studies

Section S8: Steady state and time resolved optical studies

Section S9: Radiative and non-radiative rate constants

Section S1: Characterization of green solvent medium

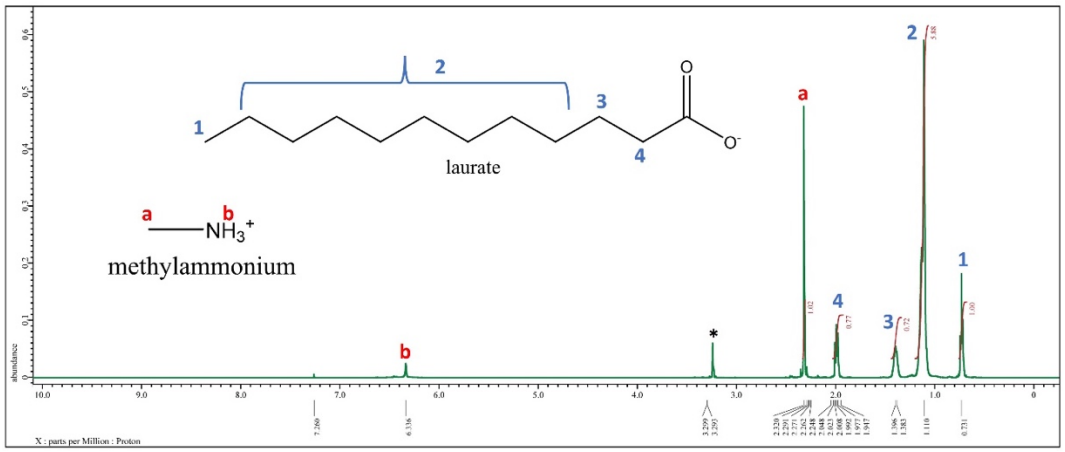

Figure S1. ^{1}H NMR spectrum of the ionic liquid like green solvent medium. (*) peak at 3.29 ppm originates from the residual methanol.

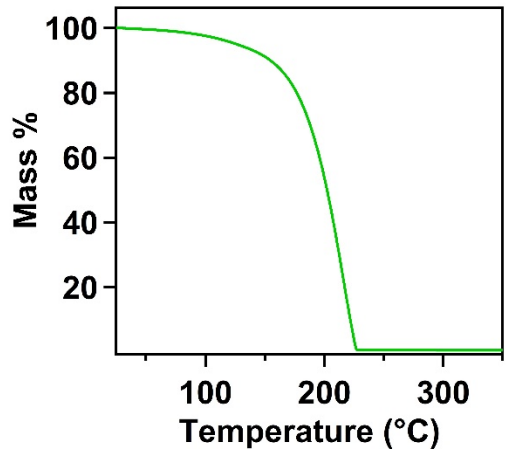

Figure S2. TGA data of the IL like green solvent medium

Section S2: Reusability of the green solvent medium

The reusability of the solvent medium was checked for ten times. $PbBr_2$ (50 mg) salt was added to the reaction medium (3 mL) to prepare $MAPbBr_3$ NCs. The NCs was then centrifuged at 40ºC and collected through redispersing in hexane. The green medium that remained in the supernatant was then again used for the synthesis of the NCs. This process was repeated for ten times and each time the NCs were prepared show more or less same PL intensity (figures S3a and S3b) and in pure cubic crystalline phase (figure S3c).

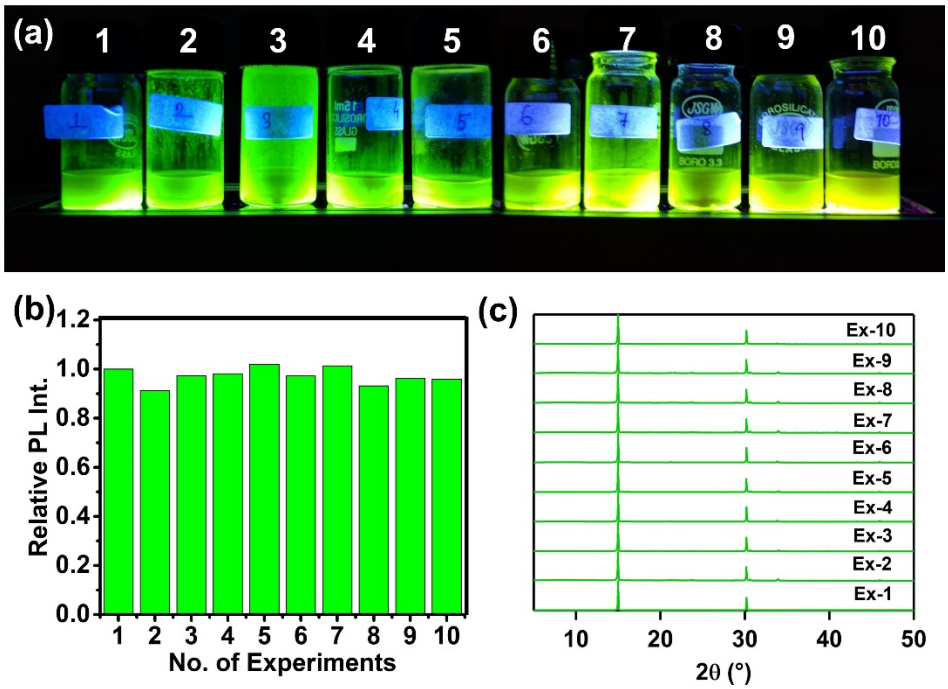

Figure S3. Reusability of the green solvent medium. (a) Optical images of the hexane extracted $MAPbBr_3$ NCs under UV light (365 nm) prepared by adding $PbBr_2$ to reused green medium (1-10 denotes the n^{th} time that green medium being reused). (b) Relative PL intensity of the $MAPbBr_3$ NCs, prepared by reusing the green medium. (c) PXRD patterns of the $MAPbBr_3$ NCs, prepared by reusing the green medium.

Section S3: Characterization of oleylammonium halide salts

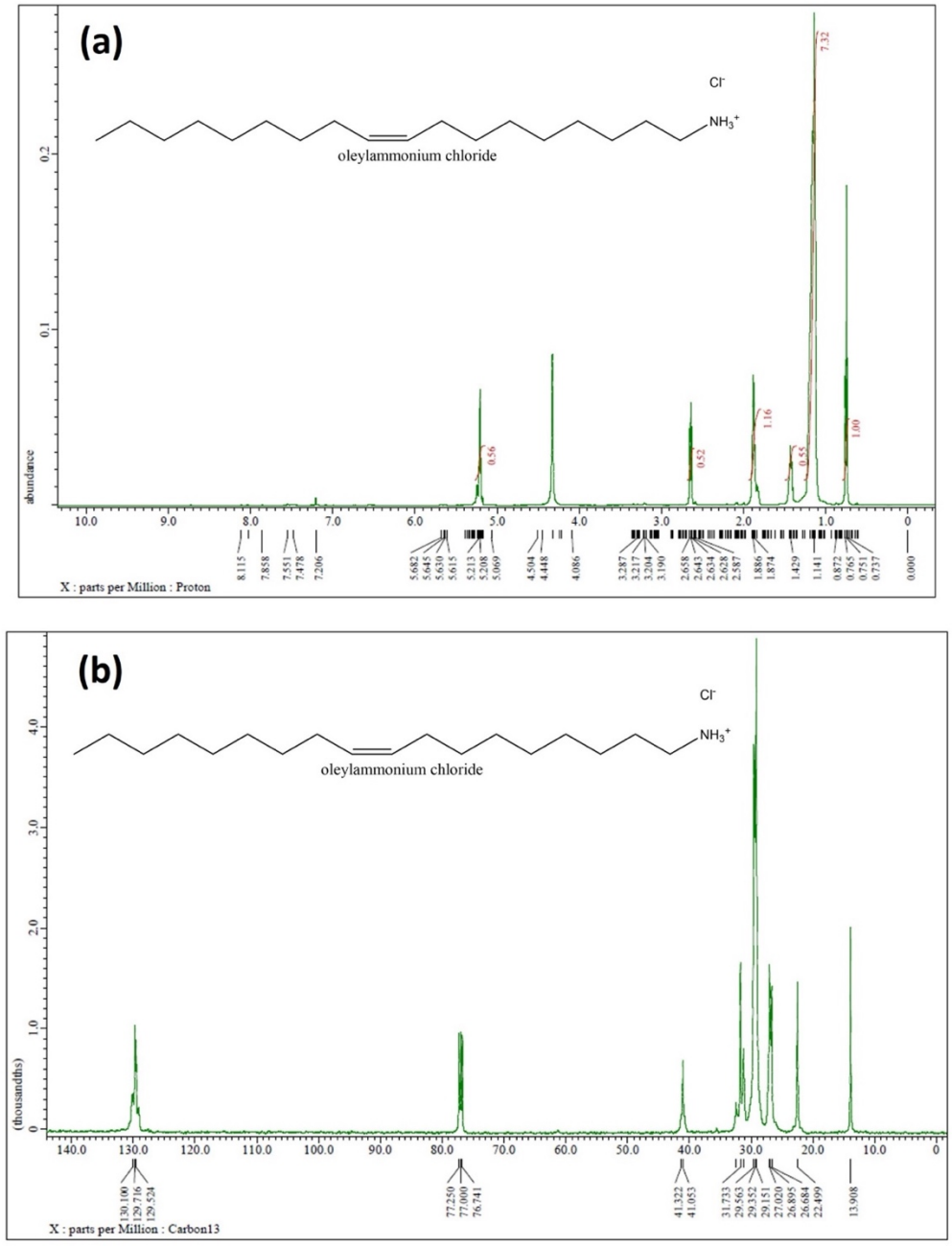

Figure S4. (a) ^{1}H NMR spectrum of OAmCl. (b) ^{13}C NMR spectrum of OAmCl.

OAmCl: ^{1}H NMR ($CDCl_3$, 500 MHz): δ 0.79 (t, 3H), 1.18 (m, 22H), 1.47 (m, 2H), 1.88-1.94 (m, 4H), 2.68 (t, 2H), 5.25 (m, 2H) (see figure S4a. Section S3 of the ESI). ^{13}C NMR ($CDCl_3$, 100 MHz): δ 14.1, 22.67, 26.87, 27.2, 29.35, 29.55, 29.75, 31.44, 31.92, 41.21, 76.94, 77.2, 77.45, 129.9 (see figure S4b. Section S3 of the ESI).

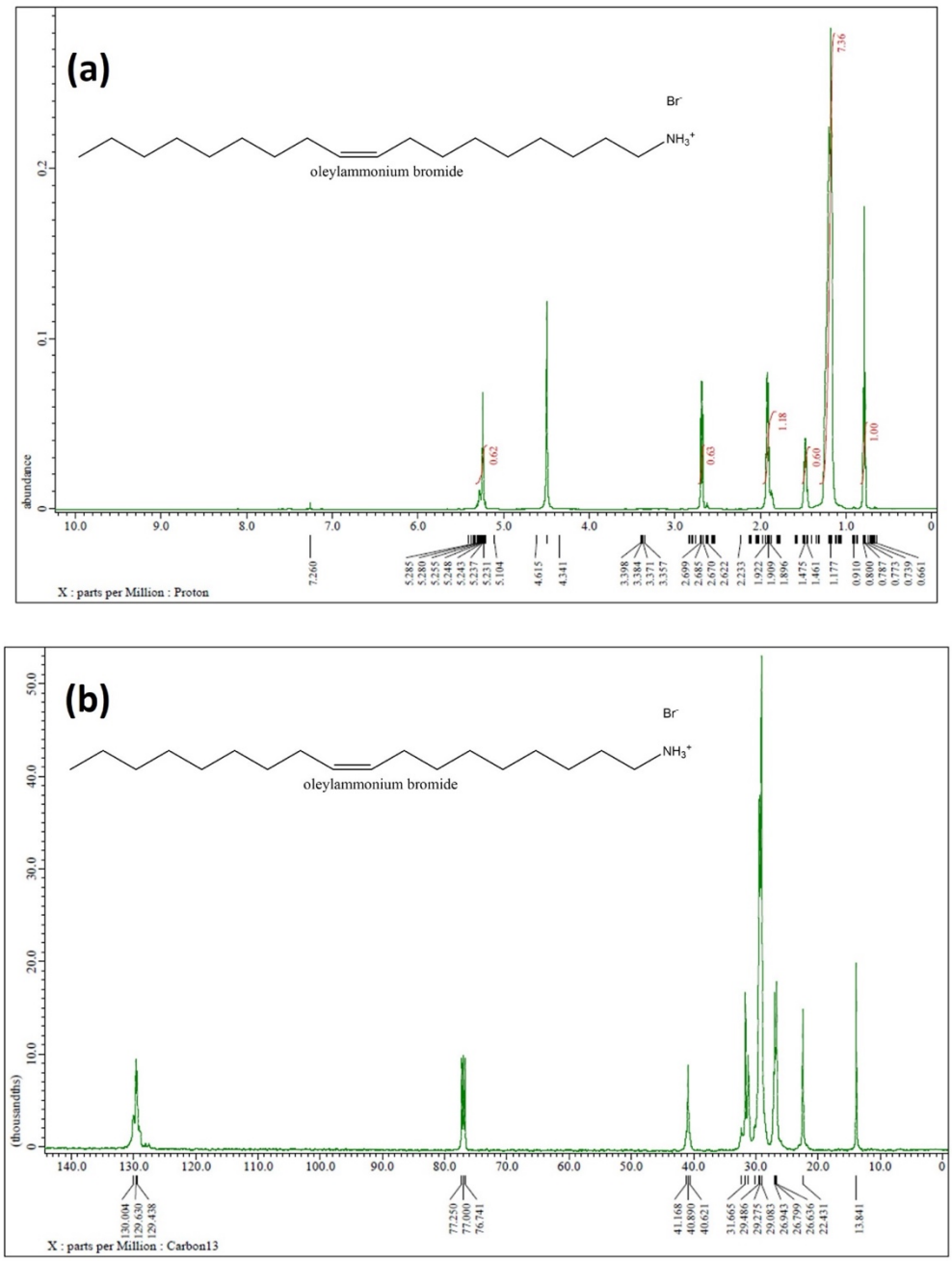

Figure S5. (a) ^{1}H NMR spectrum of OAmBr. (b) ^{13}C NMR spectrum of OAmBr.

OAmBr: ^{1}H NMR ($CDCl_3$, 500 MHz): δ 0.77 (t, 3H), 1.16 (m, 22H), 1.46 (m, 2H), 1.86-1.93 (m, 4H), 2.67 (t, 2H), 5.26 (m, 2H) (see figure S5a. Section S3 of the ESI). ^{13}C NMR ($CDCl_3$, 100 MHz): δ 13.8, 22.43, 26.67, 26.8, 29.01, 29.27, 29.49, 31.65, 40.89, 76.72, 77.0, 77.25, 129.7 (see figure S5b. Section S3 of the ESI).

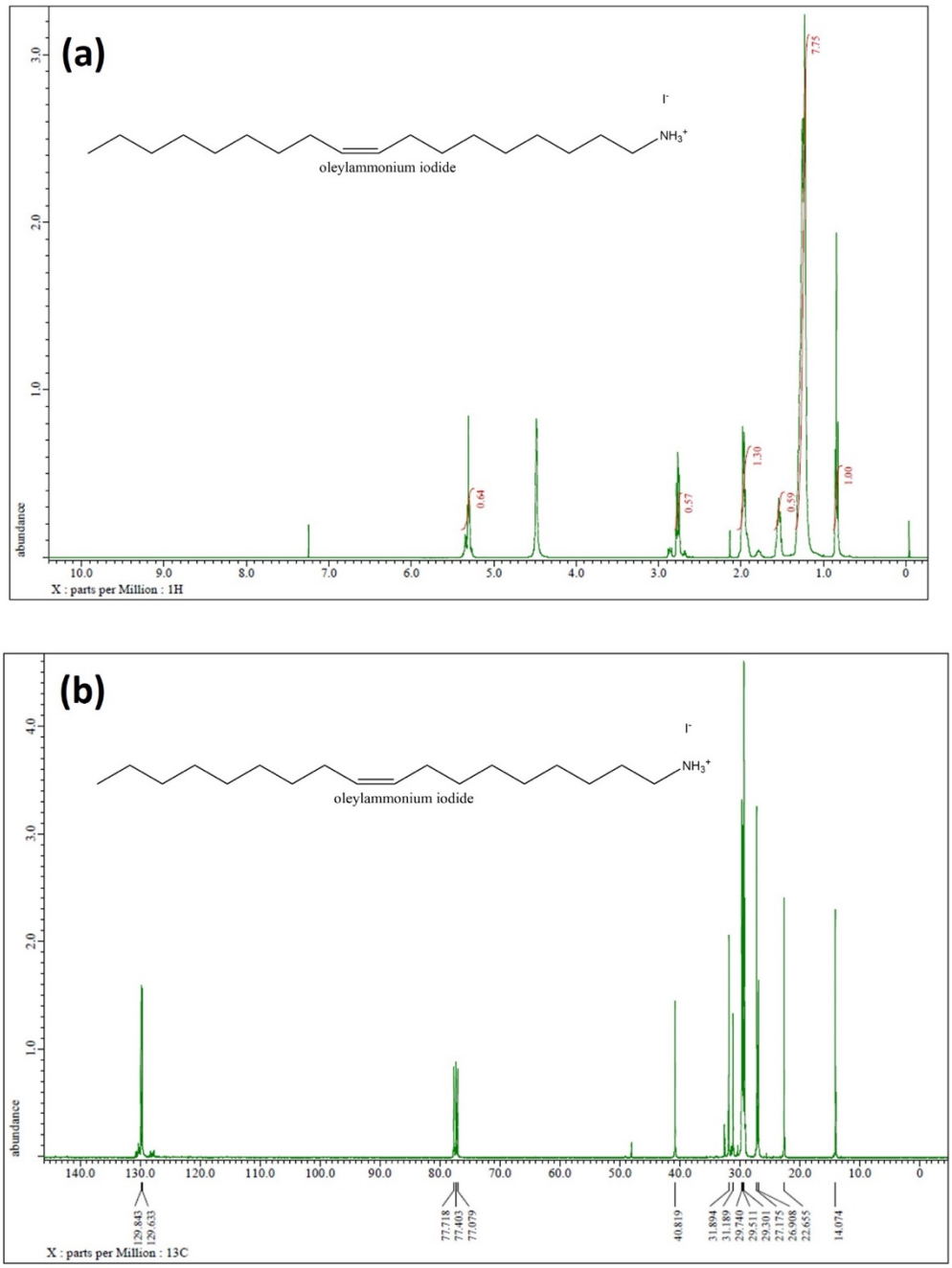

Figure S6. (a) ^{1}H NMR spectrum of OAmI. (b) ^{13}C NMR spectrum of OAmI.

OAmI: ^{1}H NMR ($CDCl_3$, 500 MHz): δ 0.84 (t, 3H), 1.23 (m, 22H), 1.44 (m, 2H), 1.92-2.01 (m, 4H), 2.77 (t, 2H), 5.31 (m, 2H) (see figure S6a. Section S3 of the ESI). ^{13}C NMR ($CDCl_3$, 100 MHz): δ 14.1, 22.64, 26.89, 27.2, 29.24, 29.51, 29.73, 31.21, 31.82, 40.77, 77.1, 77.4, 77.7, 130.2 (see figure S6b. Section S3 of the ESI).

Table S1. Percentage yield of the synthesized OAmX salts

Salt	Yield
OAmCl	87%
OAmBr	78%
OAmI	73%

Section S4: Photoluminescence quantum yield calculation

The quantum yield is estimated by comparison method by fluorescence quantum yield standard, coumarin 152A in acetonitrile, using the following equation.[S1]

$$QY(sample) = QY(ref) \times \frac{I_{sample}}{I_{ref}} \times \frac{A_{ref}}{A_{sample}} \times \left(\frac{\eta_{sample}}{\eta_{ref}}\right)^2$$

In the above equation, I_{sample} is the integrated area under the PL spectrum of the sample, I_{ref} is the integrated area under the PL spectrum of the reference solution (i.e. coumarin 152A in acetonitrile), A_{ref} is the absorbance of the refence solution at the PL excitation wavelength (400 nm), A_{sample} is the absorbance of the sample at the sample wavelength and η_{sample} (1.375) & η_{ref} (1.344) are the refractive index of the sample and reference, respectively.
The literature value of the QY of coumarin 152A in acetonitrile is 21%.[1] Using the above equation the PLQY of $MAPbBr_3$ and $MAPbBr_3$@lead laurate NCs are estimated to be 19% and 96%, respectively, upon exciting at 400 nm. Note that these PLQY values could be underestimated as the absorption of both the NCs have scattering due to their large size, which is unavoidable.

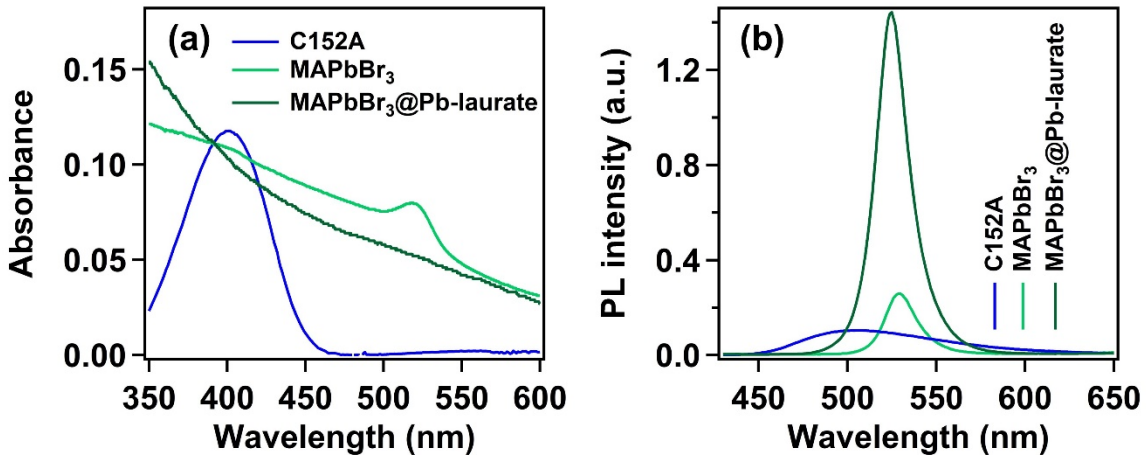

Figure S7. Quantum yield calculation data. (a) Absorption spectrum of coumarin 152A in acetonitrile, hexane suspension of $MAPbBr_3$ NCs and hexane suspension of $MAPbBr_3$@lead laurate. (b) PL spectrum of coumarin 152A in acetonitrile, hexane suspension of $MAPbBr_3$ NCs and hexane suspension of $MAPbBr_3$@lead laurate.

Section S5: Powder X-Ray diffraction studies

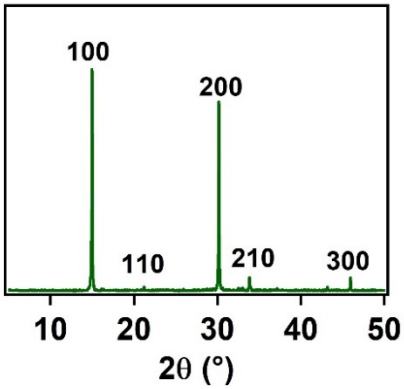

Figure S8. PXRD pattern of the purified $MAPbBr_3$ NCs. The indexing of the peaks has been done according to ref S2

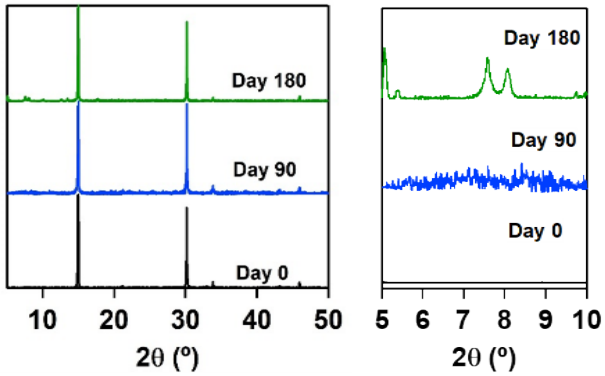

Figure S9. PXRD patterns of $MAPbBr_3$ NCs in different days after preparation.

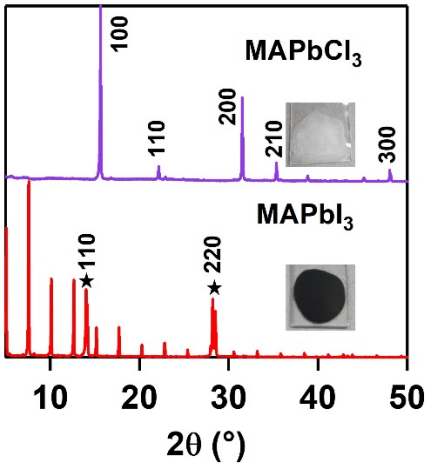

Figure S10. PXRD of $MAPbCl_3$ NCs (violet) and $MAPbI_3$ NCs (red). Both the NCs were prepared by direct addition of $PbCl_2$ salt and PbI_2 salt to the green solvent medium followed by extraction in hexane. The photographic images of the used NC films used for PXRD are given in inset.

Section S6: XPS studies

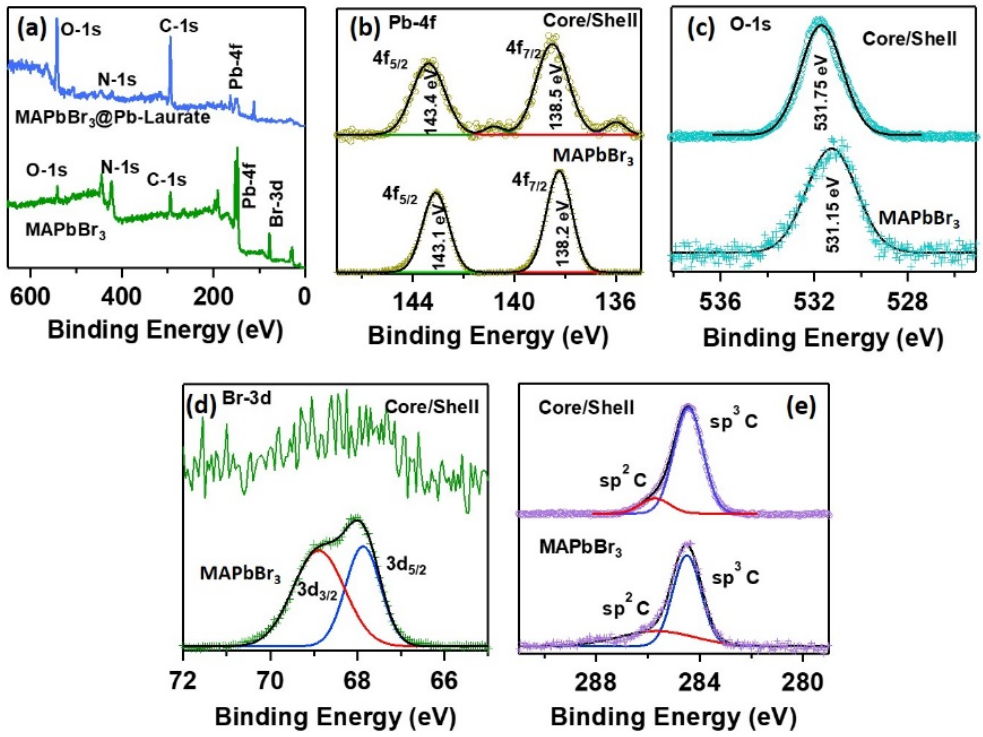

Figure S11. Comparative XPS studies of $MAPbBr_3$ NCs and $MAPbBr_3$@lead laurate core/shell nanostructure. (a) XPS survey spectrum of $MAPbBr_3$ NCs (lower part) and $MAPbBr_3$@lead laurate core/shell nanostructure (upper part). (b) High resolution XPS of Pb-4f of $MAPbBr_3$ NCs (lower part) and $MAPbBr_3$@lead laurate core/shell nanostructure (upper part). (c) High resolution XPS of O-1s of $MAPbBr_3$ NCs (lower part) and $MAPbBr_3$@lead laurate core/shell nanostructure (upper part). (d) High resolution XPS of lead-4f of $MAPbBr_3$ NCs (lower part) and $MAPbBr_3$@lead laurate core/shell nanostructure (upper part). (e) High resolution XPS of C-1s of $MAPbBr_3$ NCs (lower part) and $MAPbBr_3$@lead laurate core/shell nanostructure (upper part).

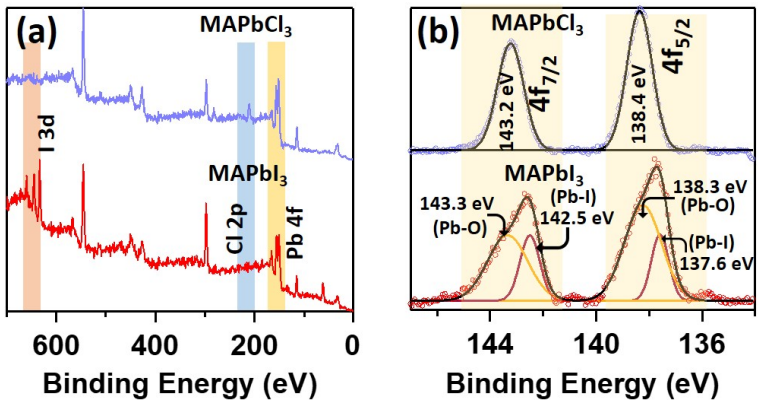

Figure S12. XPS analysis of $MAPbCl_3$ NCs and $MAPbI_3$ NCs. Both the NCs were prepared by direct addition of $PbCl_2$ salt and PbI_2 salt to the green solvent medium. (a) Survey spectra of $MAPbCl_3$ NCs (upper part, violet) and $MAPbI_3$ NCs (lower part, red). (b) High resolution XPS of Pb-4f of $MAPbCl_3$ NCs (upper part, violet) and $MAPbI_3$ NCs (lower part, red).

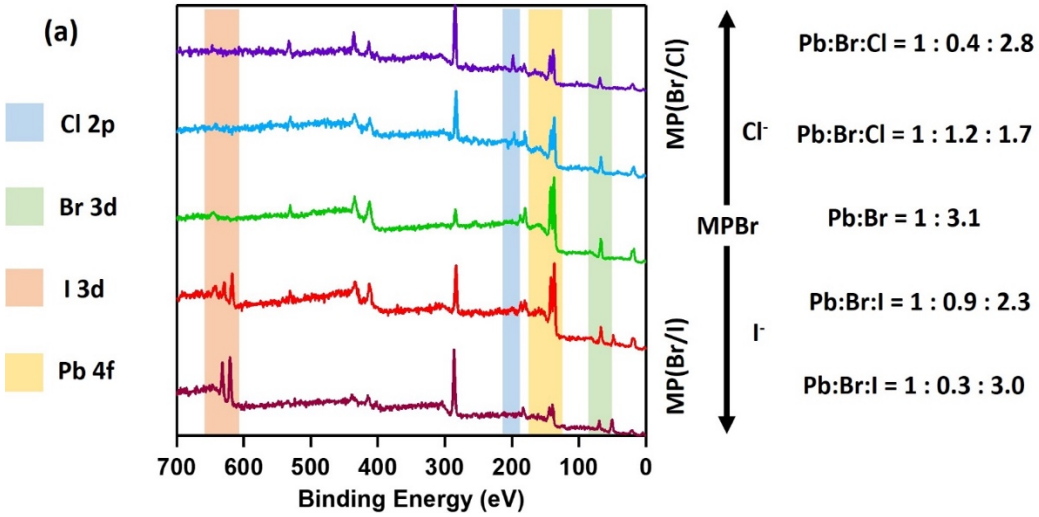

Figure S13. XPS of lead halide perovskites obtained from anion exchange reaction by OAmX (X=Cl, Br). (a) Survey spectra of lead halide perovskites obtained from anion exchange reaction by OamX. The spectra corresponding to the lead halide perovskites having PL maxima 721 nm, 652 nm, 525 nm ($MAPbBr_3$), 458 nm and 424 nm (from down to up) respectively.

Section S7: Microscopic studies

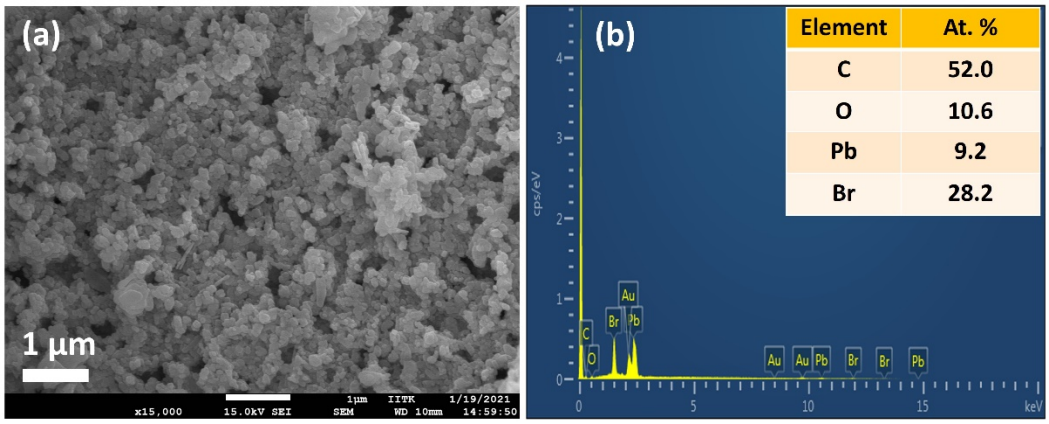

Figure S14. Scanning electron microscopic characterization of $MAPbBr_3$ NCs. (a) FESEM image of $MAPbBr_3$ NCs. (b) EDS elemental analysis of the $MAPbBr_3$ NCs from FESEM.

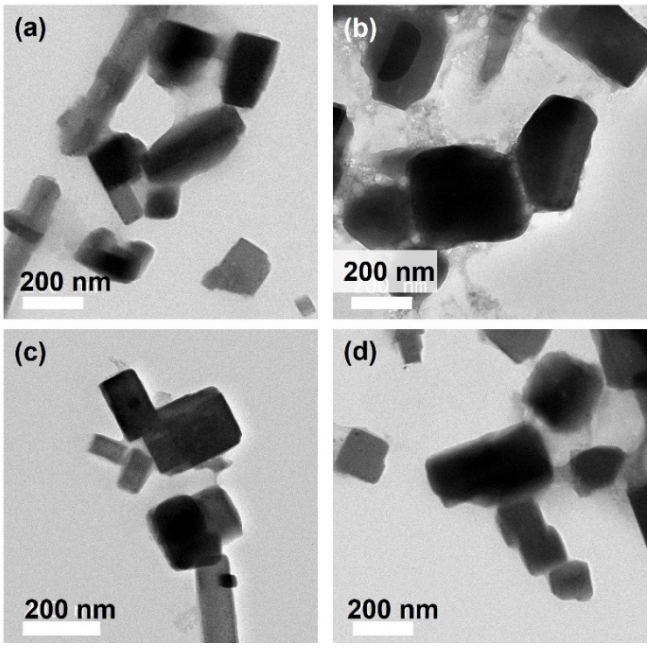

Figure S15. Additional TEM images of the synthesized $MAPbBr_3$ NCs.

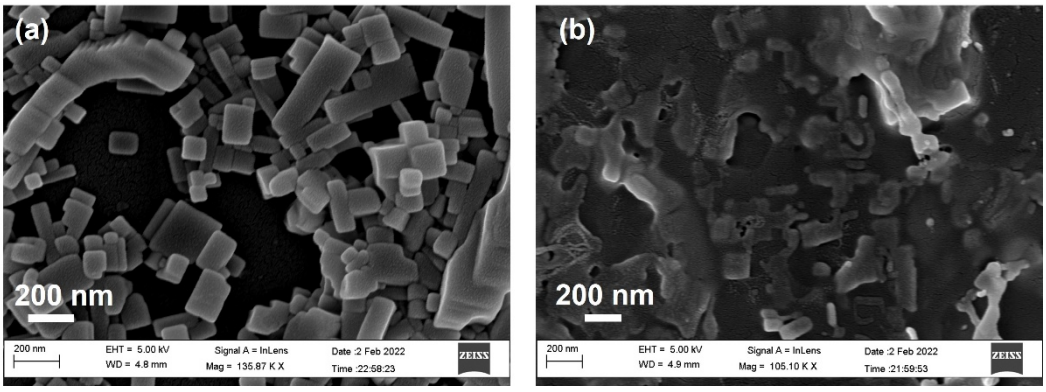

Figure S16. FESEM images of (a) $MAPbCl_3$ NCs and (b) $MAPbI_3$ NCs.

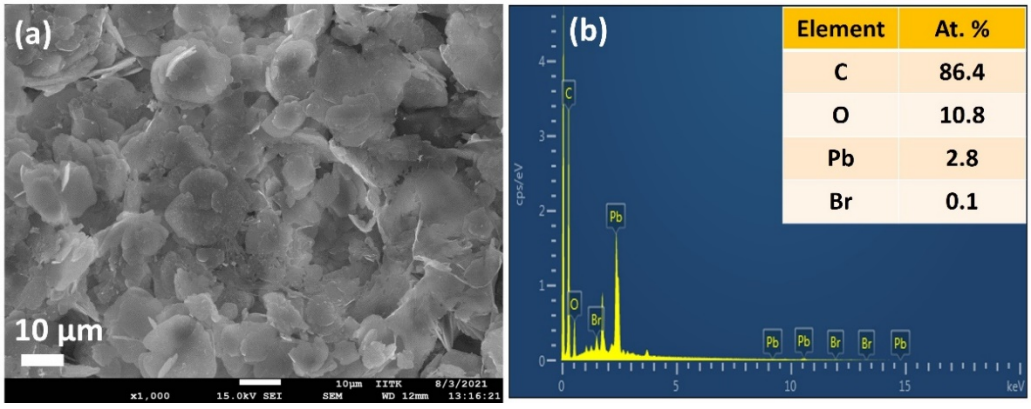

Figure S17. Scanning electron microscopic characterization of $MAPbBr_3$@lead laurate core/shell nanostructure. (a) FESEM image of $MAPbBr_3$@lead laurate core/shell nanostructure. (b) EDS elemental analysis of the $MAPbBr_3$@lead laurate core/shell nanostructure from FESEM.

Section S8: Steady state and time resolved optical studies

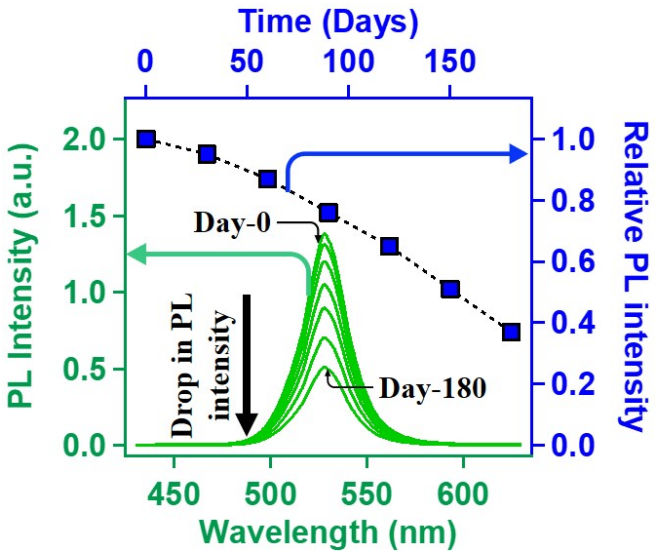

Figure S18. PL Stability of $MAPbBr_3$ NCs. The green spectra denote the original PL spectra collected at different days after preparation (Excitation wavelength is 400 nm). The blue points denote the relative change in PL intensity of the green spectra.

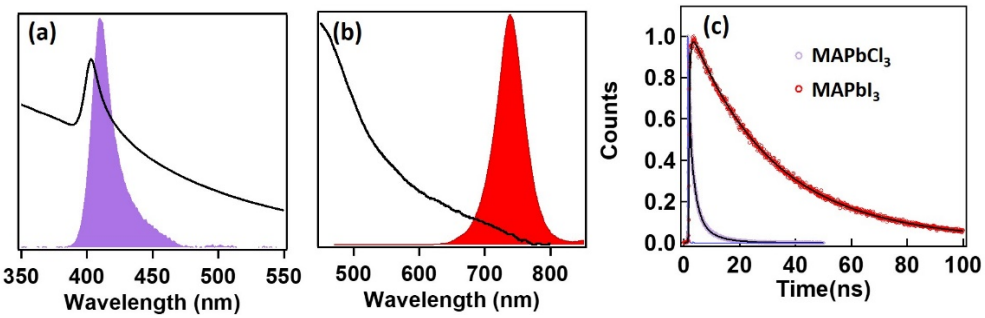

Figure S19. (a) Absorption (black) and PL spectra (violet) of $MAPbCl_3$ NCs. (b) Absorption (black) and PL spectra (red) $MAPbI_3$ NCs. (c) Time resolved PL of $MAPbCl_3$ NCs (violet) and $MAPbI_3$ NCs (red) having average lifetime 1.6 ns and 23.2 ns respectively.

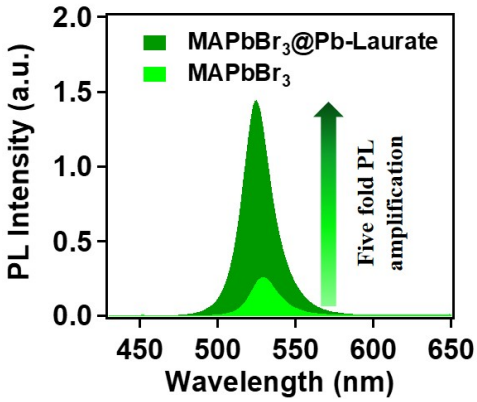

Figure S20. Comparative PL intensities of $MAPbBr_3$ NCs and $MAPbBr_3$@lead laurate core/shell nanostructure.

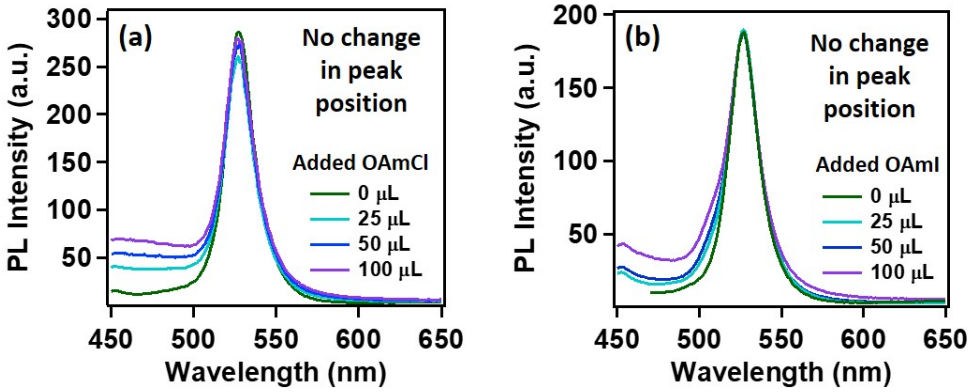

Figure S21. Response of the $MAPbBr_3$@lead laurate to the anion exchange reaction. (a) Response of the $MAPbBr_3$@lead laurate to the OAmCl. (b) Response of the $MAPbBr_3$@lead laurate to the OAmI.

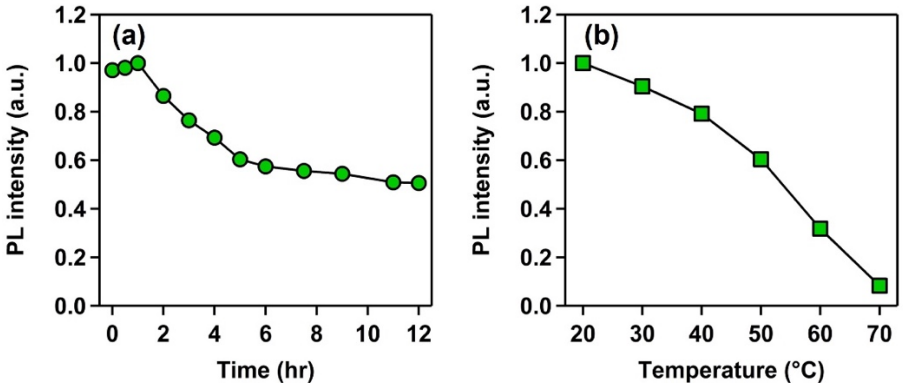

Figure S22. (a) Photostability of $MAPbBr_3$@lead laurate core-shell NCs under continuous irradiation of UV light, 365 nm, 6W. (b) Thermal stability of the $MAPbBr_3$@lead laurate core-shell NCs.

Section S9: Radiative and non-radiative rate constants

The radiative and non-radiative rate constants were calculated for both $MAPbBr_3$ NCs and core-shell NCs using PLQY and lifetime data. We know

$$PLQY = \frac{k_r}{k_r + k_{nr}} \quad \text{(S1)}$$

$$\frac{1}{\tau} = k = k_r + k_{nr} \quad \text{(S2)}$$

Where, k is the overall excited state rate constant, k_r and k_{nr} are the radiative and non-radiative rate constants, respectively.

For $MAPbBr_3$ NCs,

PLQY is 0.19 and τ is 13.6 ns.

Using the equations S1 and S2 we get,

$k_r = 1.4\times10^7\ s^{-1}$

$k_{nr} = 5.9\times10^7\ s^{-1}$

And, for the core-shell system,

PLQY is 0.95 and τ is 24 ns.

Using the equations S1 and S2 we get,

$k_r = 3.9\times10^7\ s^{-1}$

$k_{nr} = 2.1\times10^6\ s^{-1}$

References:

S1. S. Nad, M. Kumbhakar, H. Pal, *J. Phys. Chem. A,* 2003, **107**, 4808-4816.

S2. H. Shen, R. Nan, Z. Jian, X. Li, *Journal of Materials Science,* 2019, **54**, 11596-11603.